JOURNAL OF GEOPHYSICAL RESEARCH, VOL. 105, NO. D23, PAGES 29,173–29,188, DECEMBER 16, 2000

A new approach to modeling tree rainfall interception

Qingfu Xiao
Hydrology Program, Department of Land, Air and Water Resources, University of California, Davis

E. Gregory McPherson
USDA Forest Service, Pacific Southwest, Western Center for Urban Forest Research and Education, Davis, California

Susan L. Ustin and Mark E. Grismer
Hydrology Program, Department of Land, Air and Water Resources, University of California, Davis

Abstract. A three-dimensional physically based stochastic model was developed to describe canopy rainfall interception processes at desired spatial and temporal resolutions. Such model development is important to understand these processes because forest canopy interception may exceed 59% of annual precipitation in old growth trees. The model describes the interception process from a single leaf, to a branch segment, and then up to the individual tree level. It takes into account rainfall, meteorology, and canopy architecture factors as explicit variables. Leaf and stem surface roughness, architecture, and geometric shape control both leaf drip and stemflow. Model predictions were evaluated using actual interception data collected for two mature open grown trees, a 9-year-old broadleaf deciduous pear tree (*Pyrus calleryana* "Bradford" or Callery pear) and an 8-year-old broadleaf evergreen oak tree (*Quercus suber* or cork oak). When simulating 18 rainfall events for the oak tree and 16 rainfall events for the pear tree, the model over estimated interception loss by 4.5% and 3.0%, respectively, while stemflow was under estimated by 0.8% and 3.3%, and throughfall was under estimated by 3.7% for the oak tree and over estimated by 0.3% for the pear tree. A model sensitivity analysis indicates that canopy surface storage capacity had the greatest influence on interception, and interception losses were sensitive to leaf and stem surface area indices. Among rainfall factors, interception losses relative to gross precipitation were most sensitive to rainfall amount. Rainfall incident angle had a significant effect on total precipitation intercepting the projected surface area. Stemflow was sensitive to stem segment and leaf zenith angle distributions. Enhanced understanding of interception loss dynamics should lead to improved urban forest ecosystem management.

1. Introduction

Natural forests' canopy interception ranges from 15% to 40% of annual precipitation in conifer stands and from 10% to 20% in hardwood stands [*Zinke,* 1967], while it may exceed 59% for old growth forests [*Baldwin,* 1938]. Canopy interception is controlled by widely variable meteorological and canopy architecture factors [*Crockford and Richardson,* 1990]. Empirical, physically based, and stochastic models have been used to study the role of different factors that influence interception. Empirical and statistical models are first-order approximations that use linear formulas to determine rainfall interception, stemflow (ST), and throughfall (TH) as constant proportions of gross precipitation (P) [*Horton,* 1919; *Kittredge,* 1948; *Helvey and Patric,* 1965; *Zinke,* 1967]. For example, *Horton's* [1919] model is:

$$\mathrm{IL} = S + Ket, \tag{1}$$

while *Kittredge* [1948] used

$$\mathrm{ST} = b_1 P - a_1, \tag{2}$$

and *Helvey and Patric* [1965] used

$$\mathrm{TH} = b_2 P - a_2, \tag{3}$$

where IL is total interception loss, S is canopy storage capacity, K is the ratio of evaporation surface to projected area, e is evaporation rate, t is time, and a_1, b_1, a_2, and b_2 are site-specific empirical (i.e., regression) parameters obtained from long-term rainfall interception measurements. This type of model fails for small rainfall depths that do not fill the surface storage capacity. The empirically derived coefficients do not account for the influence of the magnitude of the rainfall event (i.e., rainfall intensity and duration) and canopy architecture on interception.

The first physically based interception models [*Rutter et al.,* 1971, 1975; *Rutter and Morton,* 1977] relied on water balance calculations for canopy surface water storage. This model

Paper number 2000JD900343.
0148-0227/00/2000JD900343$09.00

considered canopy surface storage as a function of gross precipitation falling on the canopy surface, drip from the canopy, and evaporation from the canopy surface and can be written

$$\frac{dC}{dt} = (1 - f_g - f_s)\, p - D_0 \exp(b\,(C - S)) - e, \qquad (4)$$

where C is canopy water storage, f_g is a gap fraction that controls the precipitation contributing to free throughfall, f_s is the precipitation fraction contributing to stemflow, and p and e are precipitation and evaporation rates, respectively. The exponential term of equation (4) represents canopy surface drip rates where D_0 and b are empirical drainage parameters and S is the canopy storage capacity. This model has been widely used in wildland forests [*Eltahir and Bras,* 1993], especially in tropical rain forests [*Jetten,* 1996], and has been modified for urban water and energy balance studies [*Grimmond and Oke,* 1991; *Xiao et al.*, 1998]. *Massman* [1983] incorporated rainfall rate into the drip component of the model using

$$d = (D_0 + d_0\, p)\,\frac{C}{S}, \qquad (5)$$

where p is rainfall rate, d is drip rate from crown leaves and stem surfaces, drip parameter D_0 is an empirical drainage constant, and the drainage parameter d_0 is determined for each event. Neither model represented by equation (4) and (5) considers canopy architecture effects on interception losses.

Gash [1979] modified the Rutter model by describing rainfall as a series of events such that the time lag between events is sufficient to dry the canopy surface. *Gash* [1979] further assumed that rainfall and evaporation rates are constant during the storm and that there is only one rain event per day. For M rainfall events that are insufficient to saturate the canopy surface completely, and N events that are large enough to completely saturate the canopy surface, Gash's model can be written

$$\sum_{j=1}^{N+M} \mathrm{IL}_j = N\,(1 - f_g - f_s)\,P' + \frac{\bar{E}}{\bar{R}}\sum_{j=1}^{N}(P_j - P') + (1 - f_g - f_s)\sum_{j=1}^{M} P_j + E_{trunk},$$

$$E_{trunk} = J\,S_t + f_s \sum_{j=1}^{M+N-J} P_j, \qquad (6)$$

$$P' = -\frac{\bar{R}S}{\bar{E}}\ln\left(1 - \frac{\bar{E}}{\bar{R}(1 - f_g - f_s)}\right),$$

where $\bar{E}$ and $\bar{R}$ are mean evaporation and rainfall rates, S_t is trunk storage capacity, and J is the number of events above the critical rainfall (S_t/f_s). Several applications of this model to interception losses in natural forests [*Pearce and Rowe,* 1981; *Gash et al.*, 1995; *Llorens,* 1997] yielded satisfactory agreement between predicted and field measurements. However, in the western United States, winter cyclonic precipitation can occur several times through the day and the short time intervals between events allow only a small fraction of canopy surface storage to be removed through evaporation.

A stochastic model developed by *Calder* [1986, 1996] used the Poisson distribution to model wetting and drying of the canopy surface. *Hall* [1992] incorporated condensation to improve model performance for high-intensity storms. Raindrop size was introduced to simulate canopy surface wetting. The model simulates the mean number of raindrops (n') retained on the canopy surface element and the mean number of raindrops (m') striking the canopy surface element through

$$n' = J'(1 - \exp(-B)) + \exp(-B)\sum_{i=1}^{M'}(i - J')\frac{B^i}{i!},$$

$$C = n'\,V_p\,L',$$

$$S = J'\,V_p\,L', \qquad (7)$$

$$B = \frac{P}{V_p L'},$$

where J' is the maximum number of raindrops that can be retained on the canopy surface element, M' is the largest integer number that is less than J', V_p is the mean volume of the raindrop, and L' is the number of surface elements per unit ground area.

More recently, *Liu* [1997] presented a combined physical-empirical model that estimates rainfall interception loss using

$$IL = S(\mathrm{DRY}_0 - \mathrm{DRY})\,[1 - (1 - f_g)\frac{\bar{E}}{\bar{R}}] + \bar{E}T, \qquad (8)$$

where DRY_0 is initial canopy dryness before rainfall, DRY is a canopy dryness index, and T is rainfall duration. Throughfall and stemflow are estimated from linear relationships with rainfall. However, the rainfall incident angle and canopy architecture were not considered.

It is difficult to apply event-based approaches to simulate the dynamic process of rainfall interception because of the large spatial and temporal variation in processes. For example, event-based models do not consider the gradual flow of water along tree stems, yet models that incorporate such factors can enhance our understanding of how interception processes impact storm runoff. An ideal interception model for tree rainfall interception should consider both meteorological and tree architectural factors that influence the interception process. The results from the model simulations, in addition to providing accurate estimation of tree interception, should be capable of distinguishing the influence of tree factors (e.g., species, architecture, dimension, shape, and leaf and stem surface roughness), rainfall factors (e.g., intensity, magnitude, and duration), and meteorological factors (e.g., wind speed, wind direction, solar radiation, and air temperature) on tree interception processes.

Nearly 80% of the United States population lives in metropolitan areas and, on average, tree canopies from about 75 billion trees cover 33% of this land area [*Johnson,* 1998; *Dwyer et al.*, 1998]. The impact of urban forests on runoff and possible flood control is of growing interest as part of efforts to protect water quality within urban watersheds. Tree planting is one of several best management practices (BMPs) demonstrated at a residential retrofit in Los Angeles [*Condon and Moriarty,* 1999]. The site has been converted into a "miniwatershed" that retains runoff on site and stores roof runoff for summer landscape irrigation. Policymakers are considering implementing this type of decentralized approach to urban watershed management, but lack quantitative data on the effectiveness of different BMPs. For instance, one need is a better understanding of how different species of trees and their spatial configuration impact runoff timing and volume at the scale of an individual tree and development parcel. Because many urban trees are open grown and relatively isolated from each other, interception data from natural forest stands may not be directly transferable to urban trees. Another need is for data to scale up from the development site to the urban watershed. Understanding and accurately estimating rainfall interception processes at the single-tree level is key to understanding rainfall interception in the urban forest.

Existing rainfall interception models have limitations to their application for estimating single-tree interception in urban environments. The primary constraint is insufficient attention to tree crown shape and structure. For example, actual rainfall interception depends less on crown projection area as seen from above than on "effective crown projection area" as seen from the angle of incoming rainfall. Effective crown projection area is influenced by tree shape. For example, Italian cypress (*Cupressus sempervirens* "stricta") is a columnar tree. Its effective crown projection area is least when the rainfall incident at zenith angle is at 0°, but increases quickly as the incident zenith angle increases to the maximum at 90°. In contrast, profusion crabapple (*Malus floribunda* "profusion") is umbrella-shaped. Its effective crown projection area is largest when the zenith angle is 0° and decreases as the incident zenith angle increases. Existing rainfall interception models do not incorporate tree crown shape or effective crown projection area.

Rainfall interception processes also depend on tree structure or architecture. For example, stemflow is greater for species with smooth bark and vertically oriented branches than for species with rough bark surfaces and horizontally oriented branches.

In this paper we present a physically based, three-dimensional, stochastic tree rainfall interception model. The model describes the interception processes at the individual tree level based on processes occurring on each single leaf and branch segment. The model accounts for rainfall, meteorological, and tree architecture factors as explicit variables derived from meteorological and tree measurement data. Results from the model simulations are compared with actual field measurements using two tree species with very different crown structures: a deciduous pear tree (*Pyrus calleryana* 'Bradford') and an evergreen cork oak (*Quercus suber*). The size and form of these trees were similar to that observed for other trees of the same species and age. Examples of the model's performance for 16 rainfall events on a deciduous pear tree and 18 rainfall events on an evergreen oak tree are provided. Because the focus is on the individual tree rather than the forest canopy, henceforth, the term "crown interception" is used.

2. Model Derivation, Parameterization, and Application

2.1. Tree Rainfall Interception Model

Assuming that there is no water absorption at the tree surface, precipitation (P) falling on crown surfaces is intercepted by crown leaf surfaces or stem surfaces, or directly passed through the leaf and stem gaps as free throughfall (Th); that is,

$$P = f_g\ P + f_l\ P + f_s\ P, \tag{9}$$

where f_g, f_l, and f_s are the fractions of precipitation becoming free throughfall, leaf surface storage, and stem surface storage, respectively. These fractions vary with rainfall incident angle and seasonal changes of tree characteristics. Change in tree surface water storage (C) is the difference between precipitation (P) and free throughfall (Th), crown drip (D), stemflow (ST), and evaporation from the tree surface (E). Symbols used hereafter are listed in the notation section.

$$\Delta \mathrm{C} = P - (\mathrm{Th} + \mathrm{ST} + D + E). \tag{10}$$

Both Th and D account for throughfall; summing Th, D, and ST yields net precipitation. C and E account for interception (I), and E accounts for interception loss (IL). Differentiating equation (10) with respect to time yields

$$\frac{\mathrm{dC}}{\mathrm{dt}} = p - f_g\ p - \mathrm{st} - d - e \tag{11}$$

where st is stemflow rate.

While equation (11) describes the water balance and interception processes at a single-tree level, more information is needed to understand these processes within the canopy. For example, a few seconds may be all that is required for water dripping off the crown surface to reach the ground, but stemflow may take several minutes to flow from branches to the bottom of the tree. Drips from leaf surfaces may fall directly to ground, or be reintercepted by stems under the leaves, suggesting that paths for throughfall and stemflow be considered separately.

To model the spatial possibilities of water flow on the tree surface, the tree crown is divided into n vertical layers. Precipitation over each layer is either intercepted by crown surfaces or directly passes through crown gaps to the ground as free throughfall. Two "reservoirs" in each layer include the leaf and stem surface storage (see Figure 1). Leaf surface storage is filled by raindrop interception and drips from upper layers, and is emptied by evaporation and dripping. Stem surface storage is also filled by raindrop interception and drips from the upper layers, as well as the water flow along the stem surface from the upper layer. The reservoir is emptied by evaporation, water flow down to the next layer along the stem surface, and drip off the stem surface. Stemflow gradually moves from tree branches to the bottom of the bole. The rainfall interception process occurs simultaneously in each layer, and the rainfall interception model flowchart is shown in Figure 2. Considering rainfall interception processes of a single layer of the tree crown, the change in storage is given by

$$\frac{\mathrm{dC_l}}{\mathrm{dt}} = f_l\ p + d_{sl} + d_{llup} - e_l - d_{l\mathrm{g}} - d_{ls} - d_{lldown} \tag{12}$$

$$\frac{\mathrm{dC_s}}{\mathrm{dt}} = f_s p + d_{ls} + d_{\mathrm{sup}} + \mathrm{st_{up}} - e_s - d_{sg} - d_{sl} - \mathrm{st_{down}} - d_{sdown}$$

where the subscripts l, s, and g represent the leaf surface, stem surface, and ground surface. The sequence of the subscripts indicates the flow direction. For example, d_{sl} here indicates the stem drip from upper layer stem surfaces to the leaf surface of this layer. The subscripts "up" and "down" indicate the upper and lower layers.

Gross precipitation falling on crown surfaces is intercepted by leaf surfaces (f_lP), and thus may become part of leaf surface storage, and by stem surfaces (f_sP), in which case it goes to stem surface water storage. The remaining precipitation directly passes through leaf gaps as free throughfall (f_gP).

For each segment of the stem at layer i, water storage is increased by intercepted rainfall, stemflow from an upper layer, and intercepted water dripping from upper layers. Water storage is decreased by evaporation and water flowing down the stem surface or dripping off the stem surface. Whether water flows to the next lower layer or drips depends on the stem segment's zenith angle. We assume that each segment is straight but that inclination varies with zenith angle. The zenith angle (θ) of these stem segments is normally distributed as $\mathrm{N}(u, \sigma^2)$ where u is the mean and σ is the standard deviation. Consider a section of a stem segment's surface in the principal flow direction. The plane is inclined at a zenith angle θ (alignment with the stem segment).

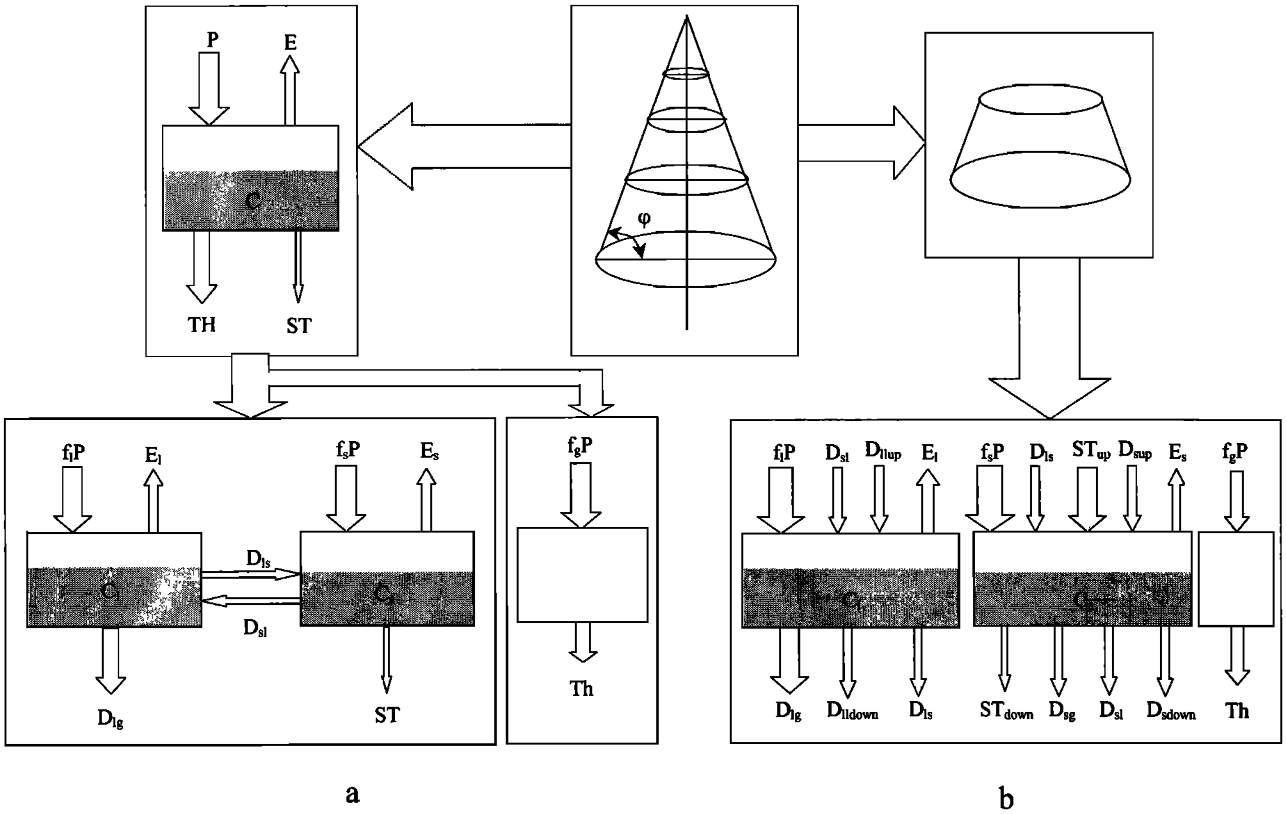

Figure 1. Rainfall interception model. (a) Rainfall interception processes at single-tree level. (b) rainfall interception at one slice of the tree crown. The crown has a cone shape with angle φ. P is the symbol for precipitation, E for evaporation, C for crown water storage, TH for throughfall, ST for stemflow, and D for the drip, and the subscripts l, s, and g indicates the leaf, stem, and ground surface.

Assume the flow is uniform at each time step Δt, that is, the depth and velocity distributions do not change with distance along the plane. Apply the momentum equation to a flow element that is bounded by the air-water interface. The element has unit width normal to the length plane, length ΔL, and depth (Y-y) from the water surface. Y is the water depth on the stem surface above detention storage. The pressure is hydrostatic across any section normal to the inclined plane because uniform flow is assumed over time Δt. In addition, the water depth is constant, and the shear stress on the water surface at the water-air interface is assumed to be negligible. Therefore the momentum equation can be written

$$W \sin\,(90^{o} - \theta) - \tau \Delta \mathrm{L} = 0.$$

Consequently,

$$\rho_w\, g\, (Y - y)\Delta \mathrm{L} \cos(\theta) = \tau \Delta \mathrm{L},$$
$$\tau = \rho_w\, g\, (Y - y)\, \cos(\theta), \qquad (13)$$

where ρ_w is the density of rainwater, τ is shear stress, g is the acceleration due to gravity, and W is the weight of the flow element. The flow velocity (v) varies with water depth on the stem surface. Because of the slow flow rate along crown stem surfaces, μdv/dy is substituted for τ such that the velocity distribution with the "no-slip" boundary condition is given by

$$\mu \frac{\mathrm{dv}}{\mathrm{dy}} = \rho_w\, g\, (Y - y)\, \cos(\theta), \qquad (14)$$

where μ is dynamic viscosity. So the discharge per unit width and the average velocity are

$$q = \int_0^Y v\mathrm{dy} = \frac{\rho_w g}{3\mu} Y^3 \cos(\theta) = \frac{g}{3\nu} Y^3 \cos(\theta), \qquad (15)$$
$$\bar{v} = \frac{g}{3\nu} Y^2 \cos(\theta),$$

where ν is kinematic viscosity.

For each layer, there are m_{stem} stem segments. Each of the m_{stem} stem segments is divided into two groups: one group for segments with inclination zenith angles less than 90° where water flows down to the next segments (Q_{down}); and a second group, with segments whose inclination zenith angles are equal to or greater than 90° from which water drips (Q_{drip}). Then the discharge from these stem surfaces can be mathematically presented as

$$Q_{downi} = \int_0^{\frac{\pi}{2}} \mathrm{CIR_i}\ \mathrm{prob}\ (\theta)\ q d\theta, \qquad (16)$$
$$Q_{dripi} = \int_{\frac{\pi}{2}}^{\pi} \mathrm{CIR_i}\ \mathrm{prob}\ (\theta)\ q d\theta$$

where $\mathrm{CIR_i}$ is the circumference of the stem surface, a function of the stem surface area and segment length. The stem surface area

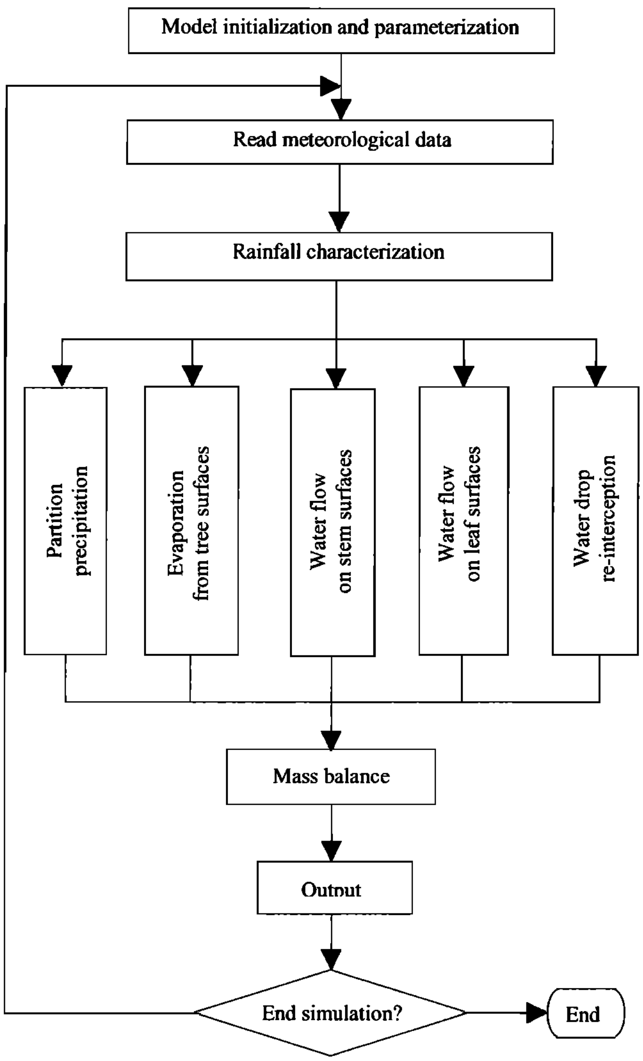

Figure 2. Tree rainfall interception model flowchart.

and zenith angle distributions are discussed in more detail in section 2.2. Thus the total water transported to the next layer is Q_{downi}, and the water that drips is Q_{dripi}. Q_{downi} adds water to the next layer's stem surface water storage. Q_{dripi} drips to the ground surface (d_{sgi}) or the layers below. There are few leaves located underneath these stems because it is assumed that all the leaves grow in the surface layer of the crown. Thus reinterception of stem drip by leaves is ignored.

An additional layer is added for modeling stemflow along the tree bole. The total throughfall contributed from stem surface drip is the sum of stem surface drip from all layers, for example,

$$d_{sg} = \sum_{i=1}^{n} d_{sgi}.$$

Thus stemflow is Q_{down} from the bole layer.

While at the single-tree level, the tree crown interception of rainfall is not like a bucket [*Massman,* 1980; *Whelan and Anderson.,* 1996]; each single leaf behaves like a tipping bucket with residual storage (saturation storage) left in the bucket. Water is stored on the leaf surface until it exceeds the maximum storage capacity. Several factors trigger water drip off leaf surfaces, including additional rainfall, water dripping from above, or wind gusts. In this case, leaf surface water storage is quickly released and water free-falls off the leaf surface. Assuming the leaves are randomly located in the crown surface and symmetrically distributed about the azimuth and zenith angle [*Verhoef,* 1984], leaf inclination distribution can be described by a two-parameter beta distribution [*Goel and Strebel,* 1984]. Consider one leaf in layer i; this leaf is presented in space characterized by zenith angle β and azimuth angle φ. Here, the azimuth angle is measured relative to the dominant wind direction. Ignoring the wind effect and applying a mass balance for the water on this leaf surface gives

$$\Delta C = P + D_{sl} + D_{llup}\ E_l - D_l, \qquad (17)$$
$$D_l = D_{lg} + D_{ls} + D_{lldown}.$$

Here, D_l is water dripping from leaf surfaces. Because the leaves are located at the crown surface, D_{llup} and D_{lldown} can be eliminated from equation (17), and taking a finite difference form yields

$$\frac{dC}{dt} = p\cos(\alpha - \beta + \frac{\pi}{2})\cos(\varphi) + d_{sl}\sin(\beta) - e_l - d_{lg} - d_{ls}, \qquad (18)$$

where α is the rainfall incident angle (zenith angle).

During a very short time period Δt, the mass of the water drip (m_p) from rainfall (p) falling to the leaf surface is

$$m_p = pA_{leaf}\cos(\alpha - \beta + \frac{\pi}{2})\cos(\varphi)\rho_w \Delta t, \qquad (19)$$

where A_{leaf} is the one-side leaf surface area. For each raindrop it is assumed that the raindrop passes all of its kinetic energy to the leaf. From conservation of momentum, the raindrop force that strikes the leaf surface (F) is

$$F\mathrm{d}t = d(m_p v), \qquad (20)$$
$$F = \frac{d(m_p v)}{\mathrm{d}t} \approx \frac{\Delta(m_p v)}{\Delta t} = -pA_{leaf}\cos(\alpha - \beta + \frac{\pi}{2})\cos(\varphi)\rho_w v,$$
$$v^2 = v_t^2 + v_w^2,$$

where v_t and v_w are the raindrop terminal velocity and wind speed. The total force applied to the leaf surface is the sum of the weight of stored water and the force caused by raindrops hitting the leaf surface. This force will determine if the leaf will tip or not. Defining a leaf rigidity factor (F_{rigid}) as the force of maximum water storage

$$F_{rigid} = A_{leaf}\ S_{\max}\ \rho_w\ g, \qquad (21)$$

where S_{max} is the leaf maximum water storage and g is gravitational acceleration. When the total force acting on the leaf surface (F_{leaf}) as a result of both the water stored and the raindrop hitting the leaf is greater than the rigidity factor, the leaf will tip. Once the leaf tips, the water storage on the leaf surface is reduced to no more than the saturation storage.

$$F_{leaf} = A_{leaf}\ Y\ \rho_w\ g + F. \qquad (22)$$

When $F_{leaf} > F_{rigid}$, this gives

$$D_l = Y + p\mathrm{d}t - S_{\min}, \qquad (23)$$

where Y is the water depth on the leaf surface at the beginning of this time step. S_{min} is the saturation storage that is the minimum amount of water required to saturate the leaf surface. Surface roughness, the finely spaced texture irregularities [*Loper*, 1987], is an important factor determining leaf saturation storage.

Maximum leaf surface water storage for individual leaves changes with the zenith angle of the leaf. When the zenith angle approaches zero, the leaf surface storage capacity reaches the minimum (S_{min}), and when the zenith angle approaches 90°, the leaf surface water storage capacity reaches a maximum (S_{max}). Assuming that S_{max} and S_{min} only vary with leaf surface roughness and leaf geometric shape, then maximum leaf surface water storage is

$$\Upsilon_{\max}(\beta) = (S_{\max} - S_{\min})\sin(\beta) + S_{\min}. \quad (24)$$

Not all of the water dripping off leaf surfaces (D_l) from layer i falls to the ground surface and contributes to throughfall (d_{lg}). Some drips are reintercepted by the stem surface at different layers underneath these leaves (d_{ls}). The magnitude of this reinterception depends on the projected effective stem surface area of the layer. Here, effective stem surface is defined as the cross-sectional area along the stem. Projecting this area onto a horizontal plane yields the projected effective stem surface area. The reinterception in layer j from this layer is calculated by

$$d_{lsj} = d_l \left(\frac{r_i}{r_j}\right)^2 \mathrm{ESPA_j}, \quad (25)$$

where r_i and r_j are the crown radii of layer i and layer j, $\mathrm{ESPA_j}$ is the effective crown projection area (defined as the stem surface area within the tree drip line) of layer j. The remainder of d_l will be reintercepted by stems below layer j until layer n, or when it finally drips to the ground surface.

Although limited evapotranspiration occurred during the rainfall events considered in our measurements, after rainfall ceases, evaporation of the wetted tree surface can occur at the potential rate. However, transpiration is restricted due to water coverage of the tree surfaces. When focusing on tree interception processes, transpiration can be ignored because this water originated from the soil. Open grown trees have limited heat storage within the crown, and the crown's ability to change wind speed and direction is also minimal. In the same environment, precipitation intercepted by vegetation evaporates at a greater rate than transpiration [*Murphy*, 1970; *Murphy and Knoerr*, 1975]. Meteorological data from the field can be directly used for estimating the potential evaporation (E_p). When crown surface water storage is below the saturation storage, evaporation from the crown surface is proportional to surface water storage [*Rutter et al.*, 1971; *Massman*, 1983; *Jetten*, 1996]:

$$E = f_{\max} E_p \frac{C}{S} \qquad C < S, \quad (26)$$

$$E = f_{\max} E_p \quad C \geq S, \quad (27)$$

where f_{max} is the fraction of maximum leaf surface wetting. E_p is estimated based on the Penman formula [*Penman*, 1948; *Xiao et al.*, 1998]:

$$E_p = \frac{\Delta}{\Delta+\gamma} Q_{ne} + \frac{\Delta}{\Delta+\gamma} E_A,$$
$$Q_{ne} = c_1 \frac{R_n}{L_e}, \quad (28)$$
$$E_A = c_2 f_e (e_a^* - e_a),$$

where Δ is the slope of saturated water vapor pressure versus air temperature, γ is the psychometric constant, Q_{ne} and R_n are net radiation in different units, E_A is drying power of the air, L_e is latent heat of vaporization of water, e_a^* and e_a are saturation vapor pressure and vapor pressure at air temperature, and c_1 and c_2 are unit constants used to convert the units. The term f_e is the wind function described by *Pruitt and Doorenbos* [1977a, b] as

$$f_e = a_u + b_u U(z) \quad (29)$$

where a_u and b_u are constants and $U(z)$ is wind speed measured at height z above ground surface. This wind function was locally calibrated and is currently used for estimating E_p in the California Irrigation Management Information System (CIMIS) network [*Pruitt et al.*, 1987; *Snyder et al.*, 1989].

2.2. Model Parameterization

There are six boundaries in the problem domain ($X\pm$, $Y\pm$, and $Z\pm$ directions). The flux of rainfall and evaporation determine the top boundary ($Z+$) condition. Throughfall (e.g., crown drip and

Table 1. Tree Architecture and Simulation Time Variables

Variable	Definition	Units[a]
	Tree Architecture	
H	tree height measured from ground surface	m
H_c	crown height measured above the first branch	m
H_b	tree bole height	m
D_c	average crown diameter which is measured in the crown principal axes directions when the crown is projected to the horizontal plane	m
DBH	diameter at breast height is the bole diameter measured at 1.3 m from ground surface	m
LAI	leaf area index, which is the ratio of the total one-side leaf surface area to the crown projection area. The maximum LAI is measured when the tree is in full-leaf. The minimum LAI is measured after most leaves fall	
SAI	stem surface area index is the ratio of the total stem surface area to the crown projection area	
f_g	gap fraction is the ratio of the total gap area inside the silhouette to the tree silhouette area. Projecting the crown to the plane that is normal to the rainfall incident angle, the outline of the crown boundary is the tree silhouette. The area inside these boundaries is the silhouette area	
CPA	crown projection area (also called normal crown projection area (NCPA)), defined as the area surrounded by the crown drip line	m^2
SPA	stem projection area, defined as the stem segment cross-section area along the stem segment surrounded by the drip line.	m^2
ECPA	effective crown projection area, defined as the CPA "seen" by rainfall	m^2
ESPA	effective stem projection area, defined as the SPA "seen" by rainfall	m^2
A_{leaf}	average leaf size, defined as one-side leaf surface area	cm^2
θ	stem segment zenith angle	deg
β	leaf zenith angle	deg
φ	leaf azimuth angle	deg
n	total number of layers into which the crown is divided	
	Simulation Time Variables	
t_{step}	time increment length or time step of the simulation	s
T_{total}	total simulation time	s

a: Units used in the model input data file.

free throughfall) and stemflow rates control the bottom boundary (Z-) condition. All water fluxes given in equation (12) are in the vertical direction; thus we assume that there is no water flux across these four boundaries of $X\pm$ (e.g., Y-Z plane) and $Y\pm$ (e.g., X-Z plane). The initial tree surface wetness is known or specified before rainfall begins.

The model required three sets of input data. The first set describes tree crown architecture: tree height, crown height, crown diameter, diameter at breast height (DBH), leaf surface area index (LAI), stem surface area index (SAI), gap fraction, leaf size, zenith angle of the stem and leaf, and surface water storage capacity of the leaf and stem (Table 1). The second set included time (Julian day, hour-minute), rainfall rate (mm h^{-1}), air temperature (°C), relative humidity (%), wind speed (m s^{-1}), wind direction (°C) and net radiation (W m^{-2}). The third input data set was user-defined and included the number of tree crown layers, the simulation time step, and the total simulation time.

Crown shape parameters affect both effective rainfall interception area and maximum surface water storage of the crown. Tree crown shape has been modeled with basic geometric solids such as spheroid, ellipsoid, parabaloid, cone, and cylinder [*McPherson et al.*, 1985; *Sattler et al.*, 1987]. Tree crown profile areas calculated using equations for geometric shapes were correlated to actual crown profile areas measured from photographs [*McPherson and Rowntree*, 1988]. Previously, a study of canopy architecture in a walnut orchard [*Martens and Ustin*, 1991; *Ustin et al.*, 1991] found that the distribution of leaves and stem surface area was related to crown diameter at different tree heights and that stem zenith angles were normally distributed. Stem surface area decreased from the bole to branch tips in Douglas fir [*Webb and Ungs*, 1993].

The following assumptions underlie parameterization of crown architecture [*Xiao*, 1998]: (1) The tree crown is multi-layered and has a perfect geometric shape; (2) Stem surface area is related to the average crown diameter and is uniformly distributed across azimuth angles for each layer; and (3) Leaves are uniformly located at the outside of the crown volume and all leaves have the same surface area, surface roughness and geometric shape.

The effective crown projection area (ECPA) differs from the normal crown projection area, taken as the area within the tree's drip line. The ECPA is the area "seen" by rainfall, so it is the area normal to the angle α of incident rainfall; that is, assuming the tree alignment is in the $Z+$ direction, the incident rainfall ECPA is

$$\mathrm{ECPA}(\alpha) = \mathrm{ECPA}_{xy} \cos(\alpha), \tag{30}$$

where ECPA_{xy} is the effective crown projection area projected in the X-Y plane. ECPA_{xy} is crown geometric shape dependent and Figure 3 illustrates how ECPA varies for a cone-shaped crown.

The tree crown gap fraction, or percentage transmission, is the ratio of gap area inside the tree silhouette to the silhouette area. It is used to describe the fraction of incident solar radiation that is transmitted through the canopy [*McPherson*, 1984]. Gap fractions reported in the literature for different tree species [*Schiler*, 1979; *Hammond et al.*, 1981; *McPherson*, 1984] were measured at varying elevation angles or on the ground. However, in rainfall interception studies, the gap fraction of the crown determines free throughfall and depends on the rainfall incident angle. Therefore it is necessary to consider how gap fractions change with different rainfall incident angles. Gap fractions measured at different incident angles on two trees were used here. The gap fractions were measured with zenith angles varying from 0° to 90° at 5° intervals [*Xiao*, 1998].

The median raindrop size for most types of rainfall can be modeled as a power function of rainfall intensity [*Laws and Parsons*, 1943; *Torres et al.*, 1994; *Uijlenhoet and Stricker*, 1999]. The median-volume diameter, D_p (mm), of the rainfall drops is related to rainfall rate, p (mm h^{-1}) by [*Laws and Parsons*, 1943]

$$D_p = 1.238 p^{0.182}. \tag{31}$$

Rainfall terminal velocity, v_t (m s^{-1}) can be determined from basic fluid mechanics. Assuming that a raindrop is released from rest, it will accelerate until it reaches the terminal velocity [*Chow et al.*, 1988]

$$v_t = \left[\frac{4gD_p}{3C_d}\left(\frac{\rho_w}{\rho_a} - 1\right)\right]^{\frac{1}{2}} \quad D_p > 0.1 \text{ mm}, \tag{32}$$

where ρ_a is the density of the air. C_d is the dimensionless drag coefficient. *Mason* [1957] defined C_d values for raindrop sizes greater than 0.1 mm. For raindrop sizes less than 0.1 mm diameter, C_d is specified by using *Stokes'* law, that is $C_d = 24/Re$ where Re is the Reynolds number.

The velocity of water drops falling on the stem surfaces from upper layer dripping is ignored because across the short distances no greater than the crown height, stem segments have much greater rigidity than leaves.

The azimuth angle of rainfall drops is associated with wind direction. The incident angle (zenith angle) of rainfall is determined from the relationship between rainfall terminal velocity (v_t) and horizontal wind speed (v_w) at half of the crown height, given by

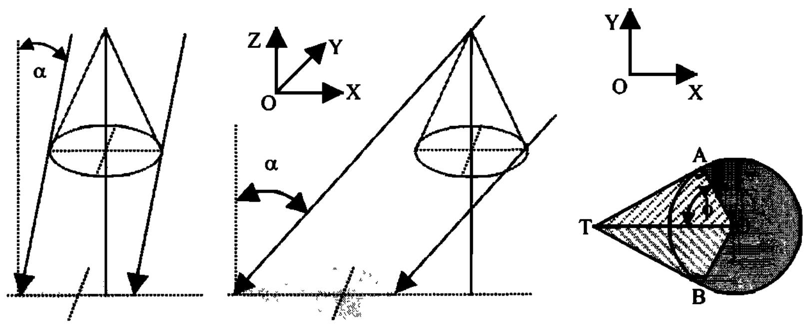

Figure 3. Effective crown projection area in an X-Y plane for a cone-shaped crown. The tree was located in the X-Y-Z space and then projected onto the X-Y plane as shown in the shadow. Here, α is rainfall incident angle.

Figure 4. Field rainfall interception measurement installation for the oak and pear trees.

$$\alpha = \arctan(\frac{v_w}{v_t}) \quad (33)$$

Here v_w is estimated from wind speed measurements on site [*Jetten*, 1996].

3. Field Experiments and Model Analysis

3.1. Field Methods

The rainfall interception experiments were conducted at the Department of Environmental Horticulture field site, in the southeast corner of the University of California, Davis campus (longitude 121°46'32" W, and latitude 38°32'09" N). On average, 90% of the average annual precipitation of 446 mm ± 36 mm occurs between November and April at the study site. No snowfall occurred in the study area. Rainfall intensity ranges from 1 to 113 mm h^{-1} and is heaviest during winter storms, which deliver most of the annual precipitation. Interception data were collected from a 9-year-old broadleaf deciduous pear tree (*Pyrus calleryana* "Bradford" or Callery pear) and an 8-year-old broadleaf evergreen oak tree (*Quercus suber* or cork oak). The pear tree and the oak tree were open grown and separated by about 63 m. The micrometeorological station was 20 m from the oak tree site and 70 m away from the pear tree site. Rainfall interception data were collected during the winter of 1996-1997 for the pear tree and during the winter of 1997-1998 for the oak tree.

A catchment was constructed below each tree to collect incident precipitation. The catchment consisted of two panels with sloping sides (angle dependent on the tree size and shape) linked together by a plastic rain gutter. The tree was located in the geometric center of the catchment. The catchment construction height was near the bottom of the crown, so that it did not influence turbulence, or vertical mixing of water vapor. The rain gutter guided water into the throughfall storage container. Using a mass balance, throughfall was determined as the difference between the water collected in the throughfall container and catchment surface detention storage, and the precipitation falling outside of the crown drip line. Stemflow was directly collected from the tree bole using a channel fabricated from a 2.54 cm diameter soft Tygon tubing that was split and spiraled around the tree bole. Gaps between the tubing and tree bole were sealed with clear 100% silicone sealant. A water container was used for storing stemflow. Gross precipitation was collected with a 15.2 cm diameter glass funnel set at the upwind corner of the catchment linked to a gross precipitation container. The water level change inside the containers was monitored using a pressure gauge (Honeywell, Inc.) and a CR10 datalogger (Campbell Scientific, Inc.). A standard micrometeorological station was established over turf grass for measuring air temperature, relative humidity, wind speed, wind direction, and net radiation. Catchment detention storage and water travel time from the catchment to the water storage container were directly measured in the field [*Xiao et al.*, 2000]. Figure 4 shows the field measurement setup.

Tree dimensions (tree height, crown height, crown diameter, DBH or diameter at breast height, and crown shape) and tree architecture data (leaf surface area, stem surface area, crown gap

Table 2. Architecture of the Oak Tree and Pear Tree

Variable	Oak Tree	Pear Tree
Tree height, m	5.6	8.5
Crown height, m	4.8	6.8
Crown diameter, m	3.2	4.8
DBH, cm	12.5	22.0
LAI, Max.	4.0	...[a]
LAI, Min.	4.0	0.0
SAI	1.7	1.7
Average leaf size, cm^2	2.4	...
Gap fraction (leaf on)	0.3	...
Gap fraction (leaf off)	0.4	0 6
Leaf zenith angle distribution, deg (minimum)	0.0	...
Leaf zenith angle distribution, deg (maximum)	160.0	...
Leaf zenith angle distribution, deg (mean)	65.0	...
Stem zenith angle distribution, deg (minimum)	0.0	0 0
Stem zenith angle distribution, deg (maximum)	120.0	120.0
Stem zenith angle distribution, deg (mean)	60.0	50.6
Leaf surface water storage, mm (maximum)	0.7	...
Leaf surface water storage, mm (saturation)	0.3	...
Stem surface water storage capacity, mm	0.8	0.6
Number of layers in crown	20	20

a: Parameters are not used for wintertime rainfall interception.

fraction, leaf and stem segment angle) were directly measured after the experiment ended. A dry weight - leaf surface area method was used to estimate the total leaf surface area from sampled leaves. The stem surface area was directly measured from each stem segment. The leaf and stem segment inclination angles were estimated using a photographic method [*Xiao*, 1998]. The gap fraction was estimated as the ratio of the gap area inside the crown silhouette area to the crown silhouette area using an image analysis technique [*Xiao et al.*, 2000]. These measured data for the pear and oak trees are listed in Table 2.

3.2. Interception Model Calibration and Sensitivity

The model equation (12) was explicitly solved using the finite difference method where numerical instability errors are reduced by limiting the maximum time step to 1 min. The error function [*Press et al.*, 1992] was used to estimate the cumulative probability distribution of equation (16). The model crown was divided into 20 vertical layers.

Two meteorological data sets and tree architectural data sets were used to calibrate the model. Only surface storage was not directly measured in the field but was adjusted via model calibration such that differences between the simulated and field measurement results were less than 10%. We assumed the tree surface was initially dry when starting simulations. Rainfall hyetographs used to drive the model calibration for the oak and pear trees are shown in Figures 5a and 5b. Figures 5c and 5d show the calibration results for both the oak tree (Figure 5c) and the pear tree (Figure 5d). For the oak tree the gross precipitation was 8.75 mm for this event as recorded at the micrometeorological station, but 8.76 mm gross precipitation fell on the crown. Similarly, for the pear tree these values were 6.05 mm and 5.93 mm, respectively. The difference in gross precipitation that fell on the tree surface is due to wind effects during the event. Wind changed the raindrop pathway from vertical, thereby changing the effective crown projection area. When we compared model results to field observations, the mean absolute percent error [*Mayer and Butler*, 1993] for all interception processes was less than 5% for the oak tree, and less than 4% for the pear tree. These differences seemed acceptable considering the measured differences in gross precipitation and that dry canopy surface was assumed when starting simulations.

A sensitivity analysis was conducted to determine the parameters having the greatest effects on interception processes. This analysis was performed using data only from the evergreen oak tree because the pear tree was dormant and leafless at the time of measurement. In the sensitivity analysis the following parameters were changed by ± 50% to assess their effect on interception: rainfall rate and duration, wind speed, LAI, SAI, gap fraction, stem and leaf zenith angle distributions, and stem and leaf surface storage capacities.

Results using the index below of the detailed sensitivity analyses are listed in Table 3a for meteorological parameters and Table 3b for tree architecture parameters.

$$\text{sensitivity\_index} = \left| \frac{\dfrac{PR_c - PR_b}{PR_b}}{\dfrac{Par_c - Par_b}{Par_b}} \right| \times 100. \qquad (34)$$

PR_c is the predicted result based on the adjusted parameter value (Par_c), and PR_b is the predicted value based on the parameter base value (Par_b).

Not surprisingly, interception processes were sensitive to rainfall rate, but less so to its duration. At a given rainfall duration, decreasing rainfall intensity by 50% caused interception loss to increase from 32% to 57% for the oak tree, or a sensitivity index of 22.7%. Decreasing rainfall intensity reduced the amount of rainwater added to the tree crown. This increased the proportion of rainwater used for wetting the crown surface, a main component of interception loss from rainfall. Increasing the rainfall rate by 50% caused the interception loss to decrease from

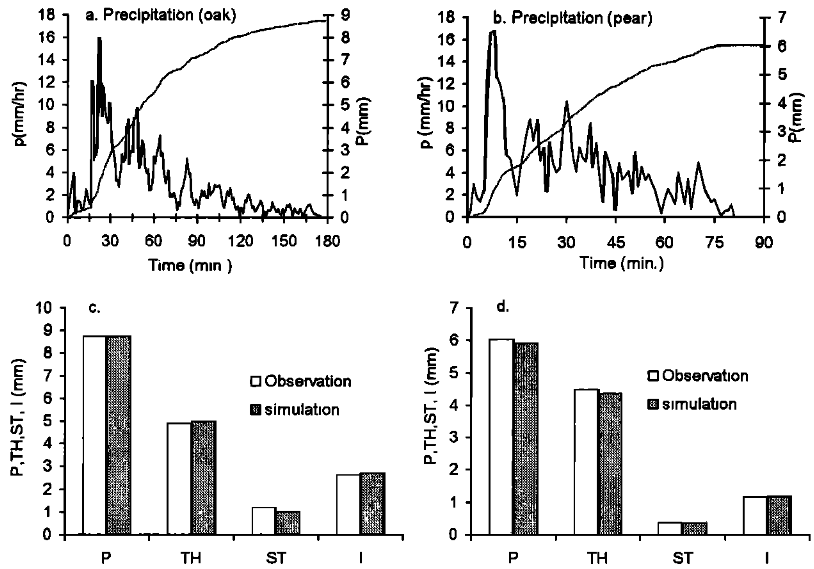

Figure 5. Calibration of the model parameters for rainfall interception processes on oak and pear trees. (a) Rainfall started at 0000:00, January 4, 1998, and it lasted about 3 hours. These data were used for the simulation on the oak tree. (b) Rainfall started at 0052:00, February 4, 1997, and it lasted about 80 min. These data were used for the simulation on the pear tree. (c) The field observation results and the simulation results are compared for the calibration on the oak tree. (d) The field observation results and the simulation results are compared for the calibration on the pear tree. P indicates cumulative precipitation, TH indicates throughfall, ST indicates stemflow, and I indicates interception loss.

Table 3a. Sensitivity Analyses Results for Meteorological Parameters

Input[a]				Output[b]				
Precipitation		Wind Speed	Gross Precipitation,	Net Precipitation				Interception Loss,
Rate	Duration		mm (%)	Stemflow, mm (%)	Free Throughfall, mm (%)	Canopy Drip, mm (%)	Total mm (%)	mm (%)
0.5	1	1	4.4 (99.1)	0.0 (200.0)	1.6 (99.0)	0.4 (160.8)	1.9 (135.5)	2.5 (22.7)
1.5	1	1	13.1 (98.4)	2.0 (219.1)	4.6 (98.4)	3.6 (174.2)	10.2 (142.2)	2.9 (5.0)
2	0.5	1	8.7 (1.6)	0.9 (6.4)	3.0 (2.0)	1.9 (1.0)	5.9 (2.7)	2.8 (0.7)
0.5	2	1	8.8 (0.9)	1.0 (3.2)	3.1 (0.7)	2.0 (1.5)	6.0 (1.5)	2.8 (0.7)
1	1	0.5	8.5 (6.8)	0.9 (17 0)	3.0 (7.2)	1.8 (10.3)	5.7 (9.7)	2.8 (1.4)
1	1	1.5	9.3 (12.3)	1.1 (31.9)	3.3 (11.7)	2.1 (20.6)	6.5 (18.2)	2.8 (0.7)
1	1	1	8.8 (...)	0.9 (...)	3.1 (...)	1.9 (...)	6.0 (...)	2.8 (...)

a: Here 1 in the input parameters indicates 1 unit, 0.5 means reduce 50%, 1.5 means increase 50%, and 2 means increase 100% from the original value. All of the canopy parameters are in 1 unit of original value

b: Output values are presented in total amount in millimeters (and in sensitivity in percentage) calculated based on equation (34).

32% to 22%, or a sensitivity of 5.0%. Using a constant rainfall depth, we tested the sensitivity of interception processes to rainfall duration. Rainfall rates were adjusted to keep the rainfall depth constant for storms of different durations. Interception processes were not as sensitive to changes in rainfall duration as compared to changes in the rainfall rate.

Interception processes were sensitive to changes in wind speed. An increase in wind speed of 50% caused gross precipitation on the canopy surface to increase by more than 6%. The sensitivity of precipitation on the tree surface, stemflow, canopy drip, net precipitation, and interception loss to increased wind speed by 50% were 12.3%, 31.9%, 20.6%, 18.2%, and 0.7%, respectively. The influence of interception loss was small compared with other process components; however, increased wind speed changed the distribution of the components.

Of all tree factors, interception loss was most sensitive to the surface area and surface water storage capacity. Changing stem surface by 50% caused a 50% sensitivity to interception loss. Increasing stem surface water storage capacity by 50% caused an 8.0% increase in interception loss. Decreasing LAI by 50% caused a 6.8% decrease in interception loss where the sensitivity is 44.7%. Increasing leaf surface water storage capacity by 50% caused a 6.8% increase in interception.

The sensitivity of interception loss to a 50% increase in gap fraction was only 12.1%. However, the distribution and proportion of throughfall and stemflow changed. The

Table 3b. Sensitivity Analyses Results for Tree Architecture Parameters

Input[a]							Output[b]					
Tree Structure					Surface Storage Capacity		Gross	Net Precipitation				Interception
Gap Fraction	LAI	SAI	Zenith Angle				Precipitation,	Stemflow,	Free Throughfall,	Canopy Drip,	Total,	Loss,
			Leaf	Stem	Leaf	Stem	mm	mm (%)	mm (%)	mm (%)	mm (%)	mm (%)
0.5	1	1	1	1	1	1	8.8	1.2 (61.7)	1.5 (102.9)	3.2 (126.8)	5.9 (2.0)	2.9 (4.3)
1.5	1	1	1	1	1	1	8.8	0.7 (57.4)	4.6 (102.3)	0.8 (118.6)	6.1 (5.4)	2.7 (12.1)
1	0.5	1	1	1	1	1	8.8	1.1 (23.4)	3.1 (0 0)	2.5 (52.6)	6.6 (20.8)	2.2 (44.7)
1	1.5	1	1	1	1	1	8 8	0.8 (21.3)	3 1 (0 0)	1.5 (44 3)	5.4 (17.8)	3.3 (36.9)
1	1	0.5	1	1	1	1	8.8	1.2 (61.7)	3.1 (0.0)	2.4 (43.3)	6.7 (23.5)	2.1 (50.4)
1	1	1.5	1	1	1	1	8.8	0.6 (72.3)	3.1 (0.0)	1.6 (38.1)	5.2 (23.9)	3.5 (49 6)
1	1	1	0.5	1	1	1	8.8	2.1 (248.9)	3.1 (0.0)	1.4 (53.6)	6 6 (21.5)	2.2 (46.1)
1	1	1	1.5	1	1	1	8.8	1.0 (4.3)	3.1 (0.0)	2.1 (19.6)	6.2 (7.1)	2.6 (15.6)
1	1	1	1	0.5	1	1	8.8	2.1 (244.7)	3.1 (0.0)	1.4 (57.7)	6.5 (19.8)	2.2 (42.6)
1	1	1	1	1.5	1	1	8.8	1.0 (4.3)	3.1 (0.0)	2.1 (19.6)	6.2 (7.1)	2.6 (15.6)
1	1	1	1	1	0.5	1	8.8	1.0 (10.6)	3.1 (0.0)	2.2 (22.7)	6.2 (8.7)	2.6 (19.1)
1	1	1	1	1	1.5	1	8 8	0.8 (23.4)	3.1 (0.0)	1.4 (52.6)	5.3 (20.8)	3.4 (43.3)
1	1	1	1	1	1	0.5	8.8	1.4 (91.5)	3.1 (0.0)	2.2 (22.7)	6.6 (21 8)	2.2 (46.1)
1	1	1	1	1	1	1.5	8.8	0.5 (89.4)	3.1 (0.0)	1.7 (21.6)	5.3 (21.5)	3.5 (44.7)
1	1	1	1	1	1	1	8.8	0.9 (...)	3.1 (...)	1.9 (...)	5.95 (...)	2.8 (...)

a: Here 1 in the input parameters indicates 1 unit, 0.5 means reduce 50%, and 1.5 means increase 50% from the original value. All meteorological parameters are in 1 unit of original value.

b: Output values are presented in total amount in millimeters (and in sensitivity in percentage) calculated based on equation (34).

sensitivities of canopy drip and stemflow to a 50% decrease in gap fraction were 126.8% and 61.7%, respectively. Stemflow was also sensitive to changes in stem/leaf zenith angle, as decreasing stem segment zenith angles by 50% caused a 13.6% increase in the amount of stemflow. This sensitivity follows because the zenith angle controls the stemflow rate and determines the water flow from one stem segment to the next segment or drip to ground surface. The sensitivity of stemflow to change in leaf zenith angle was 248.9% for a 50% decrease in leaf zenith angle. Increasing the leaf zenith angle caused more water to flow from the leaf to stem surfaces, thereby increasing stemflow.

4. Results and Discussion

We applied the model to 16 rainfall events for the broadleaf deciduous tree (pear) and 18 rainfall events for the broadleaf evergreen tree (oak) with meteorological and tree architecture parameters determined from field measurements. A minimum 4 hour period of no precipitation was used to differentiate one rainfall event from the next. The amount of precipitation intercepted by the tree surface, stemflow, throughfall, and interception losses are expressed in depth units with respect to normal crown projection area.

Figure 6 shows a comparison of field measurements versus simulated estimates of rainfall, throughfall, stemflow, and interception loss for both the oak (Figures 6a – 6d) and pear (Figures 6e – 6h) trees. There was relatively good agreement between measured and estimated values, as R^2 values ranged from 0.84 to 0.99. The difference in measured and estimated precipitation striking the tree crown was relatively small for both the oak and pear trees (Figure 6a and 6e). Throughfall was only slightly underestimated for the oak tree (Figure 6b), but overestimated for the pear tree (Figure 6f), as indicated by the slightly negative and positive intercepts of the regression lines. Stemflow was underestimated for both the oak (Figure 6c) and

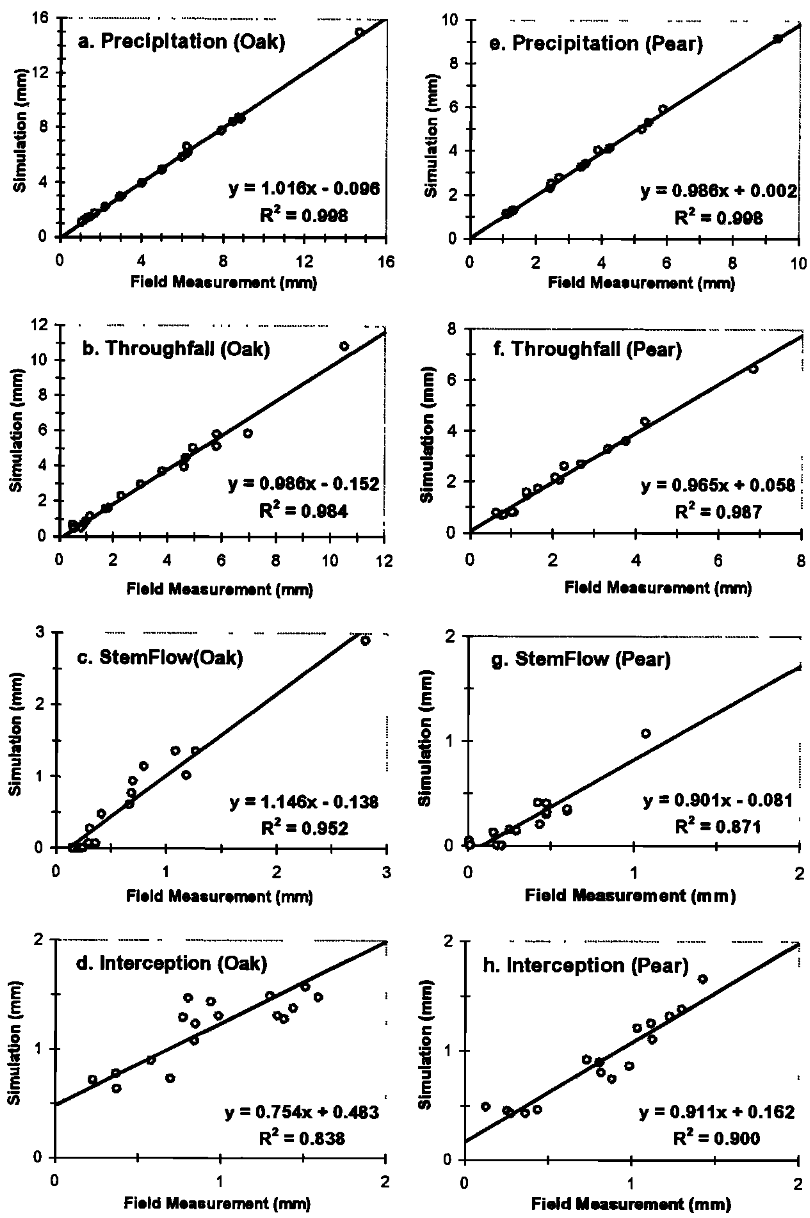

Figure 6. Field measurement and numerical simulation results of rainfall, throughfall, stemflow, and interception loss on the (a-d) oak and (e-h) pear trees. The solid line in each plot is the best fit regression line.

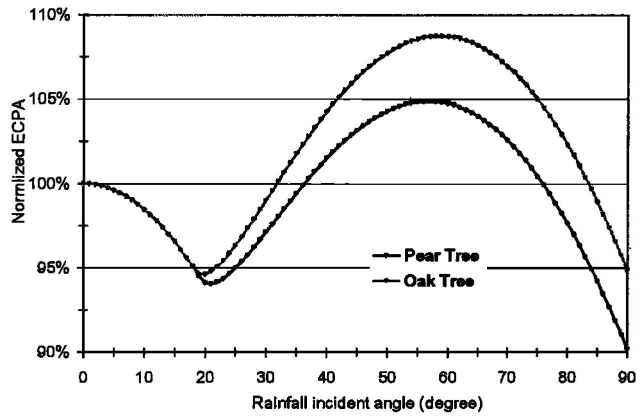

Figure 7. Effective crown projection area (ECPA) varies with incident rainfall angle. The vertical axis presents the normalized ECPA value, which is the ratio of ECPA to the normal crown projection area. The minimum ECPA existed when incident rainfall angle was 20.0° for the oak tree. The pear tree's ECPA reaches a minimum value at 21.0° incident rainfall angle.

pear trees (Figure 6g). Interception losses were overestimated in simulation for both the oak and pear trees (Figures 6d and 6h). We consider these processes and differences individually in the following paragraphs.

Use of the ECPA to standardize the input precipitation determines the amount of precipitation available for interception by the crown surface. Both wind speed and rainfall rate determine the incident angle of rainfall as well as the ECPA. Thus the model simulation of precipitation that fell over the effective crown surface was different from the amount of precipitation that fell over the normal crown projection surface. For example, on January 3, 1998 (between 2059 and 2318), 6.2 mm of gross precipitation was recorded at the micrometeorological station, but the model simulation for the oak tree indicated that 6.6 mm of gross precipitation fell on the tree crown when referenced to normal crown projection area. This 0.4 mm increase (6.5%) in gross precipitation on the tree surface was caused by the wind's changing the raindrop pathway from vertical, thereby increasing the ECPA relative to the normal crown projection area. Figure 7 shows how rainfall incidence angle affected the ECPA for the oak and pear trees. When rainfall incident angle is greater than zero and less than 32° for the oak tree and less than 36° for the pear tree, the ECPA was less than the normal crown projection area. The ECPA quickly increased when rainfall incident angle was larger than 21° for the oak tree and 22° for the pear tree. For the 18 rainfall events used in the rainfall interception simulation for the oak tree, the meteorological station recorded total precipitation of 91.2 mm, but the model simulation indicated 91.0 mm of rainfall onto the oak tree crown. For the 16 rainfall events on the pear tree, 54.7 mm of precipitation was recorded at the meteorological station, and 54.0 mm was predicted by the model.

The simulated average interception losses were 3-4% greater than measured values. For the 16 rainfall events measured on the pear tree, the predicted interception was 26.6% of gross precipitation, while the field-measured value was 23.6%. Similarly, of the 18 rainfall events on the oak tree, the average simulated interception loss (25.0% of gross precipitation) was 4.5% higher than the field-measured value (20.5% of gross precipitation). The model predicted pear tree 7.1% stemflow on average as compared to 10.4% in the field. Throughfall for the pear tree was nearly the same as that measured (66.3% versus. 66.0%). Free throughfall accounted for 95.7% and drip from branch or stem surfaces only accounted for 4.3% of total throughfall. In contrast, for the oak tree, throughfall and stemflow values were 3.7% and 0.8% lower than observed values, respectively. Free throughfall accounted for 62.0% of the total throughfall for the oak tree, while the remainder was crown drip. Evaporation was only 0.8% of gross precipitation for the oak tree and 1.1% for the pear tree. Simulation accuracy was evaluated using mean prediction error, its standard deviation (STD), and root-mean-square error (RMSE), and these results are summarized in Table 4. Prediction accuracy was similar for both trees.

Considering model predictions for individual rain events, we illustrate in Figure 8 interception processes for the pear and oak trees during one rainfall event. For the leafless pear tree (Figure 8a), not surprisingly, free throughfall was the main component of total throughfall. Water intercepted by stem surfaces of the pear tree flowed down the trunk and became stemflow. Canopy drip was significant for the evergreen oak tree. Rainfall intercepted by the oak tree began to drip off leaf surfaces after saturation (Figure 8b). Drip from canopy surfaces continued after the rainfall stopped. Figures 9a and 9b show the rainfall hyetograph and field-measured and simulated throughfall for the oak (Figure 9a) and pear trees (Figure 9b). Free throughfall was the principal component of total throughfall, and its temporal variation followed the rainfall pattern. The smoother curve for the field data and the shift in time between field-observed and simulated data were caused by the travel time delay (approximately 1.5 min and 0.5 min for the pear tree and oak tree, respectively) for throughfall moving from the catchment to the measurement devices.

Initial surface wetness conditions explain some of the differences between measured and simulated results. While the model assumed that leaf and stem surfaces' water storage was zero, in reality the canopy surface did not entirely dry in the four hour interval due to low evaporation rates. Hence for events starting soon after a 4 hour interval, antecedent moisture increased stemflow and throughfall relative to values predicted by the model. The wetness of the crown surface at the start of rainfall affected the temporal pattern of the interception processes. For example, simulated stemflow begins 5 and 10 min earlier for the oak tree if we assume an initial crown wetness of 50% and 95% compared to a dry crown (Figure 10).

Data used for the simulation are from field measurements. The crown shape of the oak tree was similar to a cone, but the

Table 4. Simulation Accuracy[a]

	Oak					Pear				
	Total		Prediction Error			Total		Prediction Error		
	Measurement	Prediction	Mean	STD	RMSE	Measurement	Prediction	Mean	STD	RMSE
Precipitation	91.2	91.0	0.1	0.1	0.1	54.7	54.0	0.0	0.2	0.2
Throughfall	60.8	57.3	0.0	0.2	0.2	36.1	35.8	0.2	0.3	0.4
Stemflow	11.7	10.9	0.1	0.1	0.2	5.7	3.8	0.0	0.2	0.2
Interception loss	18.7	22.8	-0.1	0.1	0.2	12.9	14.4	-0.2	0.2	0.3

a: Units in millimeters. STD denotes standard deviation, and RMSE denotes root-mean-square error.

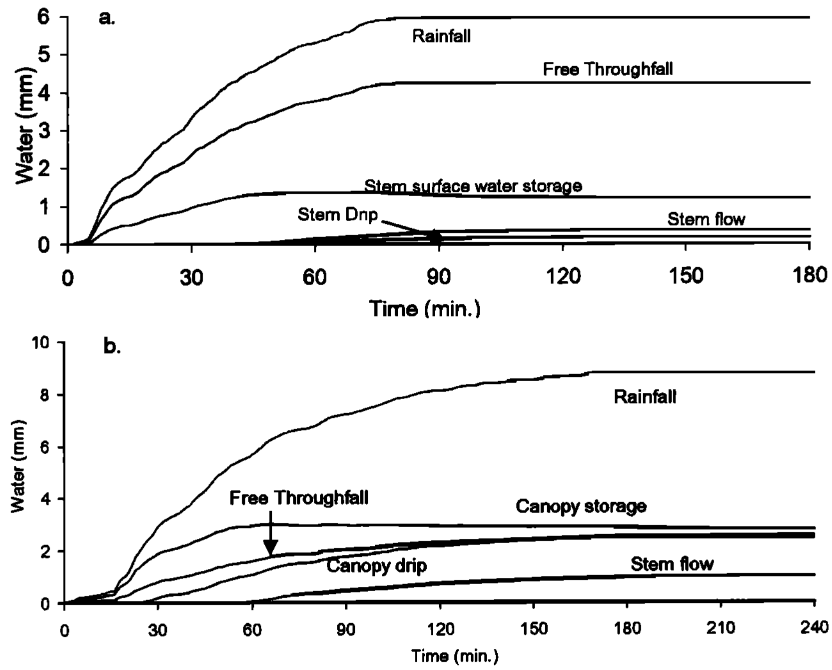

Figure 8. Rainfall interception processes. (a) Rainfall interception on the pear tree started at 0000:00, January 4, 1998, and it lasted about 3 hours. (b) Rainfall interception on the oak tree started at 0052:00, February 4, 1997, and it lasted about 80 min.

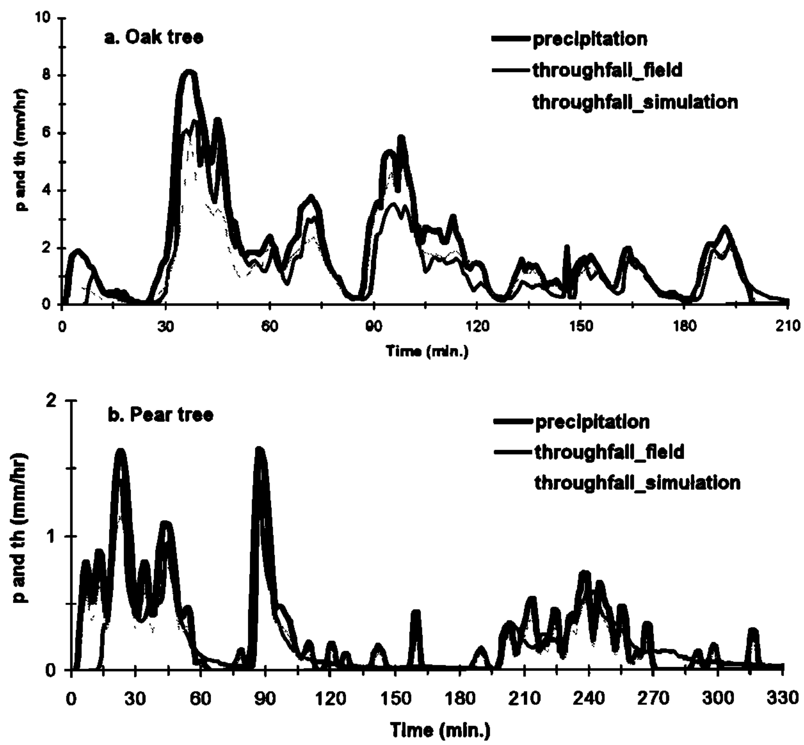

Figure 9. Rainfall interception processes. (a) Rainfall on the oak tree started at 1556, January 6, 1998, and lasted about 3 hours and simulated throughfall started at the same time. Field-observed throughfall started 7 min later. This delay is mainly caused by detention storage and water travel time on the measurement devices. (b) Rainfall on the pear tree started at 130, January 12, 1997, and it lasted about 14 hours without a break longer than 4 hours. We present 5.5 hours of data to show processes at high temporal resolution. Simulated throughfall was observed to start at the same time as rainfall, but the field-observed throughfall started 10 min after rainfall started, again, showing the detention storage and water travel time delay.

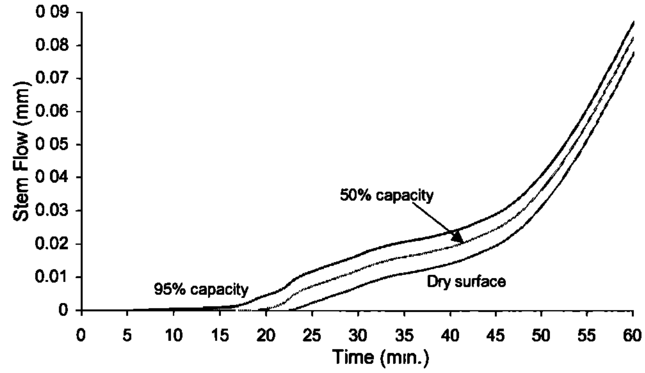

Figure 10. Influence of previous canopy surface wetness on interception processes.

bottom section of the pear tree crown was more like an ellipsoid. In the model we assumed that the crown shape of both trees was a cone. One source of estimation error may be caused by differences in crown shape.

Although this model can enhance understanding of rainfall interception processes at different temporal scales, meteorological conditions, and tree architectures, it has several limitations.

1. The model was developed for rainfall interception of open grown trees in urban settings. It cannot be directly used in rural forests where trees are influenced by nearby trees.
2. A data set for describing tree architecture is needed as model input. Obtaining these data requires intensive field measurements.
3. Wind blowing on the leaves and stems can break the equilibrium and cause water to drip from the leaf and stem surfaces. In most situations the wind does not result in tipping of a leaf, but changes the zenith angle, thereby reducing the water storage of the leaf. The wind can exert force on the leaf itself and/or on the layer of water on the leaf. This model accounted for wind effects on evaporation, but not on reducing surface water storage. Relations between wind speed and leaf zenith angle have not been established, and determining these relations was beyond the scope of this study.
4. Snow and fog interception are not included in the model.

5. Conclusions

A numerical model for predicting rainfall interception processes in open grown urban trees was developed and tested using field measurements for cyclonic-type storms on pear and oak trees. Comparison of results from the field measurements and simulations indicated that the model correctly predicted rainfall interception for both types of trees. From the model sensitivity analysis, crown rainfall interception loss was most sensitive to rainfall depth and crown surface storage capacity, followed by leaf area index and stem surface area index. Stem and leaf zenith angles are the most important factors influencing stemflow. Wetness of the crown surface at the onset of rainfall also affects interception processes.

This model provides a new tool for scientists and managers interested in better understanding rainfall interception of single trees in urban settings. Currently, statistical models provide long-term average data for interception components (e.g., gross precipitation, throughfall, stemflow, canopy storage, and interception loss), but they do not reveal the dynamic processes within storm events. This model's high temporal resolution can be used to investigate how interception influences watershed time of concentration, an important parameter in urban flood control.

Unlike other physically based rainfall interception models, the model presented in this paper more fully considers tree architecture and meteorological factors. The model's high resolution and accuracy can be useful for evaluating impacts of interception on runoff volume during less extreme events. Small storms, for which urban forest interception is greatest, are responsible for most annual pollutant washoff [*Chang et al.*, 1990]. Because the model incorporates parameters that describe important differences in tree architecture among species, it can be used to identify species that will intercept the most rainfall for regions of the country with different rainfall patterns.

The diverse species mix and heterogeneous structure of urban forests create a unique challenge to hydrologists and community foresters. Models that accurately simulate interception, runoff, and other hydrologic components at the site scale are needed because storm water management controls are shifting from point sources to dispersed, non point sources. This model provides a new method for understanding and estimating rainfall interception for such urban trees.

Notation

Rainfall

α rainfall incident angle (zenith angle) [deg].
p precipitation rate [mm h^{-1}].
P gross precipitation [mm].
v_p rainfall terminal velocity [m s^{-1}].
D_p median raindrop diameter [mm].

Tree

f_g gap fraction.
f_s stem surface interception coefficient.
f_l leaf surface interception coefficient.
f_{max} maximum fraction of leaf surface wetting.
C surface water storage [mm].
S surface water storage capacity [mm].

Climate

T_{air} air temperature, measured at 1.5 m above ground surface [°C].
RH relative humidity.
W_s wind speed [m s^{-1}].
W_d wind direction (reference to north) [deg].
$U(z)$ wind speed at height z above ground surface [m s^{-1}].
R_n net radiation [W m^{-2}].

Water flow

TH throughfall [mm].
ST stemflow [mm].
Th free throughfall [mm].
E evaporation [mm].
d drip rate [mm s^{-1}].
q stemflow rate [mm s^{-1}].
IL interception loss [mm].
e evaporation rate [mm s^{-1}].
D crown drip [mm].
S_{max} maximum surface water storage [mm].
S_{min} minimum surface water storage [mm].
S_t trunk storage capacity [mm].
D_0 empirical drainage parameters.
b empirical drainage parameters.
$\overline{E}$ mean evaporation rate [mm s^{-1}].

$\overline{R}$ mean rainfall rate [mm s^{-1}].
d_0 drainage parameters, determined from each event
st stemflow rate [mm s^{-1}].

Miscellaneous
g gravity acceleration constant [m s^{-2}].
ρ water density [kg m^{-3}].
T time [s].
τ shear stress [N m^{-2}].
μ dynamic viscosity [N s m^{-2}].

Acknowledgments. We thank William J. Massman (the Rocky Mountain Station of USDA Forest Service) and Gui-Ling Wang (the School of Engineering of the Massachusetts Institute of Technology) for their helpful comments and suggestions for improving this manuscript. This research was supported in part by funds provided by the Pacific Southwest Research Station, Forest Service, U.S. Department of Agriculture.

References

Baldwin, J. I., Interception of snowfall by forests, *For. Notes 6* (mimeo), N. H. For. and Recreat. Dep., Concord, 1938.

Calder, I. R., A stochastic model of rainfall interception, *J. Hydrol., 89*, 65-71, 1986.

Calder, I. R., Rainfall interception and drop size - Development and calibration of the two-layer stochastic interception model, *Tree Physiol., 16*, 727-732, 1996.

Chang, G., J. Parrish, and C. Souer, The first flush of runoff and its effect on control structure design, report, 33 pp., Environ. Resour. Manage. Div. Dep. of Environ. and Conserv. Serv., City of Austin, Austin, Tex., 1990. 36 pp.

Chow, V. T., D. R. Maidment, and L. W. Mays, *Applied Hydrology*, McGraw-Hill, New York, 1988.

Condon, P., and S. Moriarty (Eds.), *Second Nature: Adapting LA's Landscape for Sustainable Living*, TreePeople, Beverly Hills, Calif., 1999.

Crockford, R. H., and D. P. Richardson, Partitioning of rainfall in a Eucalypt forest and pine plantation in southeastern Australia, I, Throughfall measurement in a Eucalypt forest: Effect of method and species composition, *Hydrol. Processes, 4*, 131-144, 1990.

Dwyer, J. F., D. J. Nowak, M. H. Noble, and S. M. Sisinni, Connecting people with ecosystems in the 21st century: An assessment of our nation's urban forests, *general technical report*, 181 pp., USDA Forest Service, North Central Forest Experiment Station, Chicago, IL, 1998.

Eltahir, E. A., and R. L. Bras, A description of rainfall interception over large areas, *J. Clim., 6*, 1002-1008, 1993.

Gash, J. H. C., An analytical model of rainfall interception by forests, *Q. J. R. Meteorol. Soc., 105*, 43-55, 1979.

Gash, J. H. C., C. R. Lloyd, and G. Lachaud, Estimating sparse forest rainfall interception with an analytical model, *J. Hydrol., 170*, 79-86, 1995.

Goel, N. S., and D. E. Strebel, Simple beta distribution representation of orientation in vegetation canopies, *Agron. J., 76*, 800-802, 1984.

Grimmond, C. S. B., and T. R. Oke, An evapotranspiration-interception model for urban areas, *Water Resour. Res., 27*, 1739-1755, 1991.

Hall, R. L., An improved numerical implementation of Calder's stochastic model of rainfall interception – A note, *J. Hydrol., 140*, 389-392, 1992.

Hammond, J., J. Zanetto, and C. Adams, Planning solar neighborhoods, 179 pp., California Energy Commission, Sacramento, California, 1981.

Helvey, J. D., and J. H. Patric, Canopy and litter interception of rainfall by hardwoods of eastern United States, *Water Resour. Res., 1*, 193-206, 1965.

Horton, R. E., Rainfall interception, *Mon. Weather Rev., 47*, 603-623, 1919.

Jetten, V. G., Interception of tropical rain forest - Performance of a canopy water balance model, *Hydrol. Processes, 10*, 671-685, 1996.

Johnson, R. V., Metropolitan and non-metropolitan area population trends, in *U.S. Bureau of the Census Current Population Report, Ser. P23-194*, Population Profile of the United States: 1997, pp. 14-15, U.S. Gov. Print. Off., Washington, D.C., 1998.

Kittredge, J., Forest influences, *Interception and Stemflow*, chap. XI, pp. 99-114, McGraw-Hill, New York, 1948.

Laws, J. O., and D. A. Parsons, The relation of raindrop-size to intensity, *EOS Trans. AGU, 24*, 452-460, 1943.

Liu, S. G., A new model for prediction of rainfall interception in forest canopies, *Ecol. Modell., 99*, 151-159, 1997.

Llorens, P., Rainfall interception by a *Pinus sylvestris* forest patch overgrown in a Mediterranean mountainous abandoned area, II, Assessment of the applicability of Gash's analytical model, *J. Hydrol., 199*, 346-359, 1997.

Loper, C. R., Foundry practice and equipment, in *Marks' Standard Handbook for Mechanical Engineers*, edited by E. A. Avallone and T. Baumeister III, 9th ed., pp. 13.2-13.9, McGraw-Hill, New York, 1987.

Martens, S. N., and S. L. Ustin, Measurement of tree canopy architecture, *Int. J. Remote Sens., 12*, 1525-1545, 1991.

Mason, B. J., *The Physics of Clouds*, 481 pp. Oxford Univ. Press, New York, 1957.

Massman, W. J., Water storage on forest foliage: A general model, *Water Resour. Res., 16*, 210-216, 1980.

Massman, W. J., The derivation and validation of a new model for the interception of rainfall by forests, *Agric. Meteorol., 28*, 261-286, 1983.

Mayer, D. G., and D. G. Butler, Statistical validation, *Ecol. Modell., 68*, 21-32, 1993.

McPherson, E. G., Energy-conserving site design, report, Am. Soc. of Landsc. Architects, Washington, D.C., 1984.

McPherson, E. G., and R. A. Rowntree, Geometric solids for simulation of tree crowns, *Landsc. Urban Plan., 15*, 79-83, 1988.

McPherson, E. G., R. Brown, and R. A. Rowntree, Simulating tree shadow patterns for building energy analysis, in *Solar 35 Conference Proceedings*, edited by A. T. Wilson and W. Glennie, pp. 378-382, Am. Sol. Energy Soc., Boulder, Colo., 1985.

Murphy, C.E., Jr., Energy sources for the evaporation of precipitation intercepted by tree canopies, Ph.D. dissertation, Duke Univ., Durham, N. C., 1970.

Murphy, C. E., and K. R. Knoerr, The evaporation of intercepted rainfall from a forest stand: An analysis by simulation, *Water Resour. Res., 11*, 273-280, 1975.

Pearce, A. J., and L. K. Rowe, Rainfall interception in a multi-storied, evergreen mixed forest: Estimates using Gash's analytical model, *J. Hydrol., 49*, 341-353, 1981.

Penman, K. L., Natural evaporatoration from open water, bare soil, and grass, *Proc. Soc. London Ser., A198*, 116-140, 1948.

Press, W. H., S. A. Teukolsky, W. T. Vetterling, and B. P. Flannery, Numerical recipes in C: The art of scientific computing, in *The Art of Scientific Computing*, 2nd ed., chap. 6.2, pp. 220-222, Cambridge Univ. Press, New York, 1992.

Pruitt, W. O., and J. Doorenbos, Background and development of methods to predict reference crop evapotranspiration (ET_0), in *Crop Water Requirements*, 2nd edition, Irrig. Drain. Pap., Appendix II, pp. 108-119, Food and Agric. Organ., Rome, Italy, 1977a.

Pruitt, W. O., and J. Doorenbos, Empirical calibration, a requisite for evapotranspiration formulae based on daily or longer mean climate data, papers presented at International Round Table Conference on "Evapotranspiration", Int. Comm. on Irrig. and Drain., Budapest, Hungary, 1977b.

Pruitt, W. O., E. Fereres, and R. J. D. Snyder, Reference evapotranspiration (ETo) for California, *Univ. Calif. Bull. 1922*, 14 pp., Davis, 1987.

Rutter, A. J., and A. J. Morton, A predictive model of rainfall interception in forests, III, Sensitivity of the model to stand parameters and meteorological variables, *J. Appl. Ecol., 14*, 567-588, 1977.

Rutter, A. J., K. A. Kershaw, P.C. Robins, and A.J. Morton, A predictive model of rainfall interception in forests, I, Derivation of the model from observations in a plantation of Corsican pine, *Agric. Meteorol., 9*, 367-384, 1971.

Rutter, A. J., A. J. Morton, and P. C. Robins, A predictive model of rainfall interception in forests, II, Generalization of the model and comparison with observations in some coniferous and hardwood stands, *J. Appl. Ecol., 12*, 367-380, 1975.

Sattler, M. A., S. Sharples, and J. K. Page, The geometry of the shading of buildings by various tree shapes, *Sol. Energy*, *38*, 187-201, 1987.

Schiler, M., Computer simulations of foliage effects on building energy load calculations, chap. VII and VIII, master's thesis, Cornell Univ., Ithaca, N.Y., 1979.

Snyder, R L., B. J. Lanini, D. A. Shaw, and W. O. Pruitt, Using reference evapotranspiration (ETo) and crop coefficients to estimate crop evapotranspiration (ETc), trees and vines, *Univ. of Calif. Leaflet 21428*, 8 pp., Davis, 1989.

Torres, D. S., J. M. Porra, and J. D. Creutin, A general formulation for rainfall size distribution, *J. Appl. Meteorol.*, *33*, 1494-1502, 1994.

Uijlenhoet, R., and J. N. M. Stricker, Dependence of rainfall interception on drop size - A comment, *J. Hydrol.*, *217*, 157-163, 1999.

Ustin, S. L., S. N. Martens, and V. C. Vanderbilt, Canopy architecture of a walnut orchard, *IEEE Trans. Geosci. Remote Sens.*, *29*, 843-851, 1991.

Verhoef, W., Light scattering by leaf layers with application to canopy reflectance modeling: The SAIL model, *Remote Sens. Environ.*, *16*, 125-141, 1984.

Webb, W. L., and M. J. Ungs, Three dimensional distribution of needle and stem surface area in a douglas-fir, *Tree Physiol.*, *13*, 203-212, 1993.

Whelan, M. J., and J. M. Anderson, Modelling spatial patterns of throughfall and interception loss in a Norway spruce (*Picea abies*) plantation at the plot scale, *J. Hydrol.*, *186*, 335-354, 1996.

Xiao, Q. F., *Rainfall interception of urban forest*, Ph.D. dissertation, Univ. of Calif., Davis, 1998.

Xiao, Q. F., E. G. McPherson, J. R. Simpson, and S. L. Ustin, Rainfall interception by Sacramento's urban forest, *J. Arboric.*, *24*, 235-244, 1998.

Xiao, Q. F., E. G. McPherson, S. L. Ustin, M. E. Grismer, and J. R. Simpson, Winter rainfall interception by two mature open grown trees in Davis, California, *Hydrol. Processes*, *14*, 763-780, 2000

Zinke, P. J., Forest interception study in the United States, in *Forest Hydrology*, edited by Sopper W. E. and H. W. Lull, pp. 137-161, Pergamon, Tarrytown, 1967.

M. E. Grismer, S. L. Ustin, and Q. F. Xiao, Department of Land, Air and Water Resources, University of California, Davis, CA 95616. (xiao@vache.ucdavis.edu)

E. G. McPherson, USDA Forest Service, Pacific Southwest, Western Center for Urban Forest Research and Education, c/o Department of Environmental Horticulture, University of California, Davis, CA 95616.

(Received January 6, 2000; revised May 8, 2000;
accepted May 24, 2000.)